AIAA SciTech Forum
6-10 January 2025, Orlando, FL
AIAA SCITECH 2025 Forum

10.2514/6.2025-1748

Microstructural Uncertainty Propagation over Meso and Macro-Scale Mechanical Properties of Aerospace Metallic Alloys

Waris Khan*, Md Maruf Billah†, and Pınar Acar‡
Virginia Tech, Blacksburg, 24061, VA, USA

The mechanical behavior of aerospace metals is pivotal for ensuring the structural integrity and reliability of aircraft components. However, the presence of inherent microstructural variability in these materials introduces uncertainties in their mechanical properties, significantly impacting the performance and safety of aerospace structures. In this paper, we explore the intricate relationship between microstructural uncertainty and its propagation on meso and macro-scale mechanical properties of a titanium-aluminum alloy, Ti-7Al. First, the uncertainty of meso-scale elastic moduli is evaluated by considering the inherent randomness of substitutional alloy atoms and the microstructural texture. Next, we develop a Finite Element (FE) framework for assessing the mechanical response of macro-scale structures, integrating micro-scale uncertainty into the FE model by sampling the elasticity modulus and Poisson's ratio for each element from the distribution of material properties at the meso-scale. A benchmark study involving a transversely loaded square plate is presented to demonstrate the efficacy of our methodology. By subjecting the FE model to varying microstructural properties, we analyze the propagation of uncertainty on displacements and stresses across the structure.

Nomenclature

σ	Stress
ε	Strain
B	Strain-displacement Matrix
D	Flexural rigidity tensor
d	Nodal displacement
F	Force vector
K	Global Stiffness Matrix
k	Element stiffness matrix
$N(x)$	Shape functions
p	Load
Q	Elasticity Tensor
u	Deflection
FEM	Finite Element Method

*Graduate Research Assistant, Ph.D. Student, Department of Mechanical Engineering, AIAA Student Member
†Graduate Research Assistant, Ph.D. Student, Department of Mechanical Engineering, AIAA Student Member
‡Associate Professor, Department of Mechanical Engineering, AIAA Member

I. Introduction

Aerospace metals, such as titanium alloys, are widely used in aircraft construction owing to their favorable mechanical properties [1, 2]. However, the performance of these materials can be significantly affected by microstructural variability, which arises from inherent defects at the micro-scale [3, 4]. Understanding how uncertainties at the microstructural level propagate to affect the mechanical properties at the meso and macro scales is essential for ensuring the structural integrity and reliability of aerospace components. This paper aims to explore the propagation of microstructural uncertainty and its impact on meso and macro-scale mechanical properties of components of Ti-7Al alloy.

The microstructural features, such as grain size, orientation, shape, and single-crystal properties, have a significant impact on the mechanical properties of Ti-7Al components. For instance, variations of microstructural texture and single-crystal properties may influence the meso-scale behavior, leading to variations in the homogenized elasticity tensor (Q) [5]. Understanding and quantifying the uncertainty associated with these microstructural features are essential for predicting the mechanical behavior of aerospace structures accurately.

For instance, the epistemic uncertainty of the molecular-level computations for the single-crystal properties was investigated by examining the inherent randomness of Aluminum atoms in the Ti-7Al alloy [6]. This was combined with the aleatoric uncertainty of microstructure-level properties to assess the overall uncertainty at the meso-scale. The uncertainty for single crystals was calculated using molecular dynamics simulations, while the microstructural texture uncertainty was analyzed using experimentally measured pole figures [7]. Numerous studies have concentrated on forecasting the unpredictability of material properties originating from phenomena at the nano and micro levels. A comprehensive investigation by Ding et al. [8] utilized molecular dynamics in conjunction with the cohesive finite element method to examine the propagation of cracks in B2-NiAl alloys. By integrating material parameters derived from molecular dynamics simulations into their cohesive element model, they successfully explored the mechanisms of crack propagation at both microscopic and macroscopic scales. In another study, Acar et al. [9] addressed the inverse problem of identifying stochasticity in microstructures through variations in material properties at the mesoscale. This was achieved by developing an analytical model for uncertainty quantification, called "AUQLin." A subsequent study by Acar et al. [10] determined the slip systems parameters of Ti-Al alloys, categorically Ti-0Al and Ti-7Al, by analyzing data from tension and compression tests. The study employed a rate-independent constitutive model for single crystals and Orientation Distribution Function (ODF) as a texture probability descriptor to thoroughly investigate the material's crystal plasticity, incorporating uncertainty quantification to account for uncertainties. Despite significant progress, uncertainty in numerical model predictions and parameters continues to affect the optimal design of microstructures under various conditions [11]. Tran et al. [12] explored the impact of microstructural uncertainties on predicting homogenized material properties in polycrystalline materials, using advanced sampling techniques such as multi-index Monte Carlo (MIMC) and multi-level Monte Carlo (MLMC). Thillaithevan et al. [3] expanded on this work by addressing material uncertainties arising from manufacturing defects in additive manufacturing. They incorporated these uncertainties into a functionally-graded lattice optimization methodology, introducing a perturbation parameter to adjust design objectives in the microstructure and accommodate a range of unpredictable material properties. While considerable advancements have been made in predicting uncertainties at the nano and micro scales, further integration with meso-scale and macro-scale phenomena remains an area for research.

Numerous approaches have been developed to incorporate uncertainties in complex engineering simulations. Probabilistic and interval-based finite element methods (FEM) have become vital for addressing uncertainties in complex engineering simulations. Stochastic FEM (SFEM), for example, efficiently models non-Gaussian uncertainties in solid mechanics, capturing mechanical variability under uniform and triangular distributions with minimal computational cost, making it well-suited for complex boundary-value problems [13, 14]. In structural stability analysis, SFEM also enhances precision for thin-walled structures prone to buckling, using random field models to account for geometric imperfections [15]. For large-scale systems, Parametric Model Order Reduction (PMOR) reduces FEM model complexity while retaining accuracy, allowing for rapid uncertainty quantification (UQ) in large-scale applications, such as helicopter airframes [16]. Interval FEM extends FEM capabilities by providing conservative reliability estimates where only interval bounds are available, rather than exact probability distributions [17]. Bayesian approaches, like Hierarchical Bayesian Modeling (HBM), enhance FEM by integrating modal data across datasets to capture structural parameter variability comprehensively [18]. Finally, tools like uqFEM exemplify UQ-FEM integration for structural analysis under uncertain natural hazards, advancing resilience-based civil engineering [19].

The most well-known sampling technique is probably the traditional Monte Carlo strategy [20, 21]. It is possible to approximate the response characteristics through repeated evaluation with different random parameter realizations. Despite being the most reliable approach, it requires a substantial amount of computing power as numerous separate

simulations must be run.

Alternative sampling methods for UQ include collocation methods, which reduce simulations through strategically placed sampling points, such as Smolyak points [22]. While efficient, collocation can become computationally intensive and unstable in high-dimensional cases [23]. Perturbation methods are highly efficient, approximating quantities around the mean with a Taylor series expansion, but they are limited to simpler, polynomial material models [24, 25]. In this work, the Monte Carlo simulation is used for its robustness to capture complex behavior.

To incorporate microstructural uncertainty into macro-scale analysis, a combination of Design of Experiments (DOE) [26] and statistical sampling are employed using the Monte Carlo method. We develop a framework that integrates micro-scale variability into FEM by sampling the elasticity tensor (Q) for each finite element from a distribution of material properties derived at the meso-scale. This approach allows us to capture the material variability and its effects on the structural performance of the component. Details on how the parameters are varied are explained in a subsequent section.

The outline of the paper is as follows. In Section II, we detail the Finite Element Method (FEM) formulation, encompassing the model, loads, boundary conditions, and the quantification of uncertainty in results using FEM. Furthermore, we demonstrate the methodology on a benchmark problem to study the propagation of meso-scale uncertainty on macro-scale properties in Section III. Based on these results, we draw conclusions in Section IV.

II. Methods

As a model problem, we consider a transversely loaded square plate composed of a Ti-7Al alloy. The governing differential equation for the laterally loaded square plate is given by:

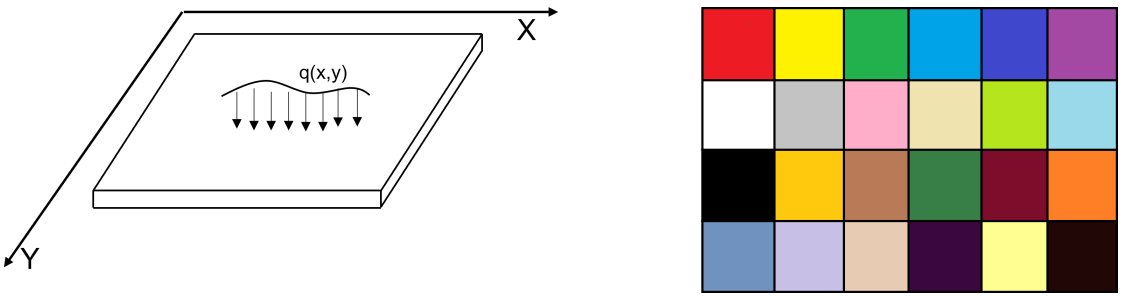

(a) **(b)**

Fig. 1 a) Square plate with distributed lateral load; b) the finite element mesh where each color represents a finite element with a different elasticity tensor

$$D\left[\frac{\partial^4 u}{\partial x^4} + \frac{\partial^4 u}{\partial x^2 \partial y^2} + \frac{\partial^4 u}{\partial y^4}\right] = p \tag{1}$$

where, u is the deflection of the plate, p is the applied load, and D is the flexural rigidity tensor of the plate. We consider two boundary conditions cases. In the first case, the plate is simply supported, resulting in zero deflection at the boundaries and allowing free rotation about axes parallel to each side. In the second case, where the plate is fixed along all edges, restricting both deflection and rotation. To solve the governing differential equation (Eq. 1) for both cases, we utilize an FEM solution.

The methodology adopted is explained in Figure 2. The probability distributions of the meso-scale properties are obtained by following the definitions of the uncertainty of microstructural texture and single-crystal properties using the formulation developed by Billah and Acar [6]. The computation of the uncertainty propagation on meso-scale properties identifies the probability distribution of elemental elasticity tensors. From this distribution, the components of the elasticity tensor are sampled.

The square plate is discretized using four-noded quadrilateral elements as shown in Figure 1b where each color symbolizes an element with a different elasticity tensor. Using this modeling technique, multiple FE simulations are performed to obtain the variations of the macro-scale properties.

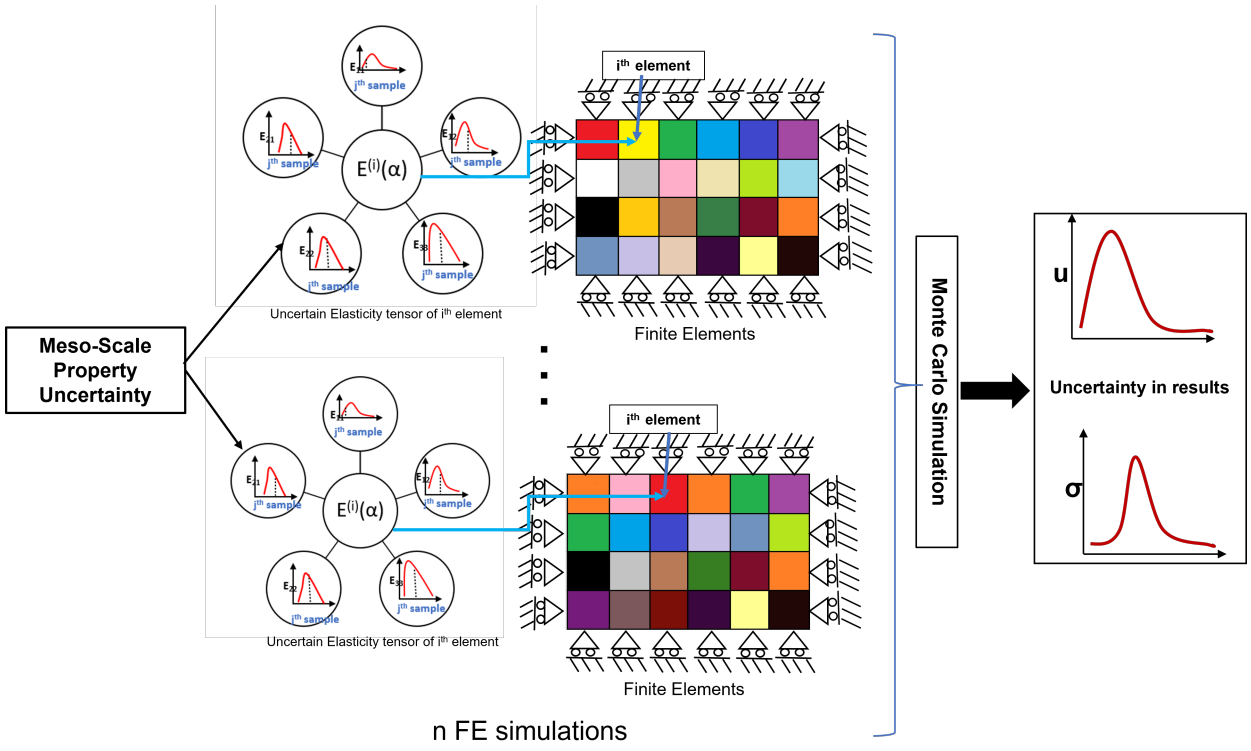

Fig. 2 Flowchart representation of the multi-scale modeling under uncertainty framework

The FE formulation for the plate includes all deterministic input parameters except for the elasticity tensor Q, which is considered a random input and sampled from the property distribution obtained at the meso-scale. The square plate is divided into finite elements, with each element having components of the elasticity tensor given by:

$$Q^{(i,j)} = \begin{bmatrix} Q_{11}^{(i,j)} & Q_{12}^{(i,j)} & 0 \\ Q_{21}^{(i,j)} & Q_{22}^{(i,j)} & 0 \\ 0 & 0 & Q_{33}^{(i,j)} \end{bmatrix} \tag{2}$$

where i represents the element number of the plate, and j represents one of the design samples from the distribution obtained for meso-scale properties. Here, j refers to a single set of design samples, which means each element's elasticity tensor Q varies according to these sampled values. This notation, (i, j), allows each finite element to have unique elasticity components sampled across the design space, aligning with the stochastic variability modeled from the meso-scale.

Let $Q(\alpha_j)^{(i)}$ be the elasticity tensor of the i^{th} element whose components are made from the j^{th} sample of the α distribution (corresponding to the distribution of $Q_{11}, Q_{12}, Q_{21}, Q_{22}$, and Q_{33} obtained as a result of the propagation of microstructural uncertainty). According to the displacement-based FE formulation, the displacement field, $u^{(i)}(x;\alpha_j)$, at some point x within the i^{th} element can be expressed as:

$$u^{(i)}(x;\alpha_j) = N^{(i)}(x)d^{(i)}(\alpha_j) \tag{3}$$

where $N^{(i)}(x)$ show shape functions corresponding to a four-noded quadrilateral element, and $d^{(i)}(\alpha_j)$ is the nodal displacement. Using Eq. 3 in the strain–displacement equations and the linear-elastic constitutive equations, the strain field, $\varepsilon^{(i)}(x;\alpha_j)$, and the stress field, $\sigma^{(i)}(x;\alpha_j)$, within the i^{th} element can be expressed as the interpolation of the nodal displacements such that:

$$\begin{aligned} \varepsilon^{(i)}(x;\alpha_j) &= B^{(i)}(x)d^{(i)}(\alpha_j) \\ \sigma^{(i)}(x;\alpha_j) &= Q^{(i)}(\alpha_j)B^{(i)}(x)d^{(i)}(\alpha_j) \end{aligned} \tag{4}$$

where $B^{(i)}(x)$ is the strain–displacement matrix. Consequently, the element stiffness matrix $k^{(i)}(\alpha_j)$ is given by:

$$k^{(i)}(\alpha_j) = \int_{V^{(i)}} B^{(i)^T}(x) Q^{(i)}(\alpha_j) B^{(i)}(x) dV^{(i)} \tag{5}$$

Furthermore, since applied loads are assumed to be deterministic, the element force vector is unaffected by uncertainties, and is given by:

$$f^i = \int_{V^{(i)}} N^{(i)^T}(x) b^{(i)}(x) dV^{(i)} + \int_{S^{(i)}} N^{(i)^T}(x) t^{(i)}(x) dS^{(i)} \tag{6}$$

where $b^{(i)}(x)$ and $t^{(i)}(x)$ are body force and traction acting on the i^{th} element, respectively. However, in this study, the body force is assumed to be zero. By assembling the global FE matrices, we obtain the following linear expression:

$$K(\alpha)U(\alpha) = F \tag{7}$$

where $U(\alpha)$ is the vector of the unknown global displacements, F is the nodal force vector, and $K(\alpha)$ is the global stiffness matrix. After formulating the FEM with randomly assigned linear-elastic properties, we perform Monte Carlo Simulations (MCS) with 100,000 samples under varying elements of the Q tensor. We then evaluate the resulting variations in displacements and stresses. The specific cases and corresponding results are discussed in detail in the following section.

III. Results

A. Benchmarking/Validation of In-House Code using ANSYS

To validate the developed FEM code in simulating macroscopic mechanical behavior, a comparative assessment is carried out using the industry-standard finite element software, ANSYS. This benchmarking ensures that the custom code produces reliable results under the specified boundary conditions and material properties.

For the comparison, an isotropic thin plate with dimensions of $20 \times 20\,\text{mm}^2$ and a modulus of elasticity of 167.2841 GPa is modeled in ANSYS using four-noded SHELL181 elements. The analysis is performed for two boundary condition scenarios: simply supported and clamped, respectively. A uniform pressure of 1 MPa is applied to the surface of the plate for both cases. The deflections and stress results are compared in the figures below.

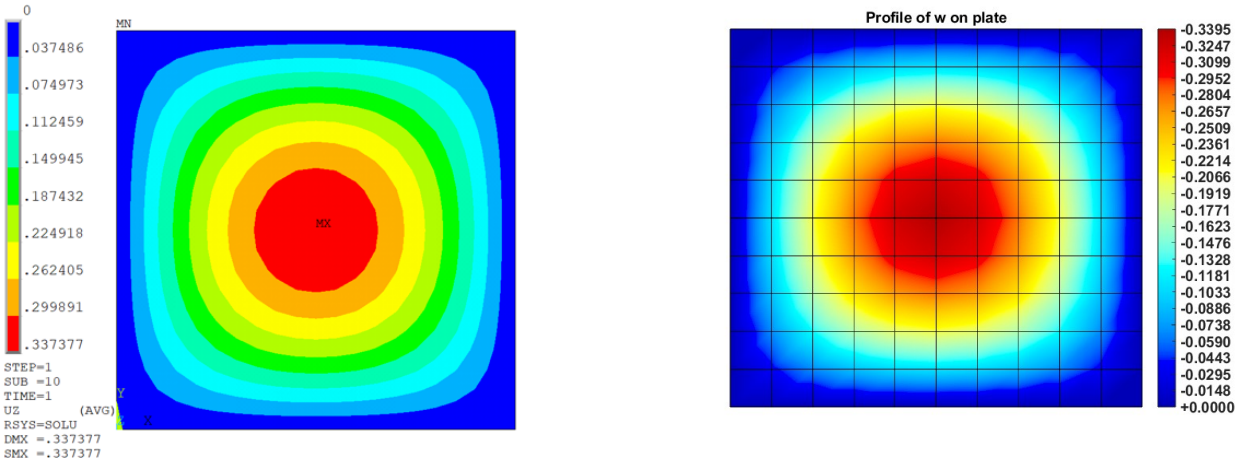

(a) **(b)**

Fig. 3 Displacement fields of the simply-supported plate acted upon by uniform pressure of 1 MPa: a) ANSYS; b) in-house code

The results in Figures 3, 4, and 5 show a close match, which validates the predictions of the in-house code.

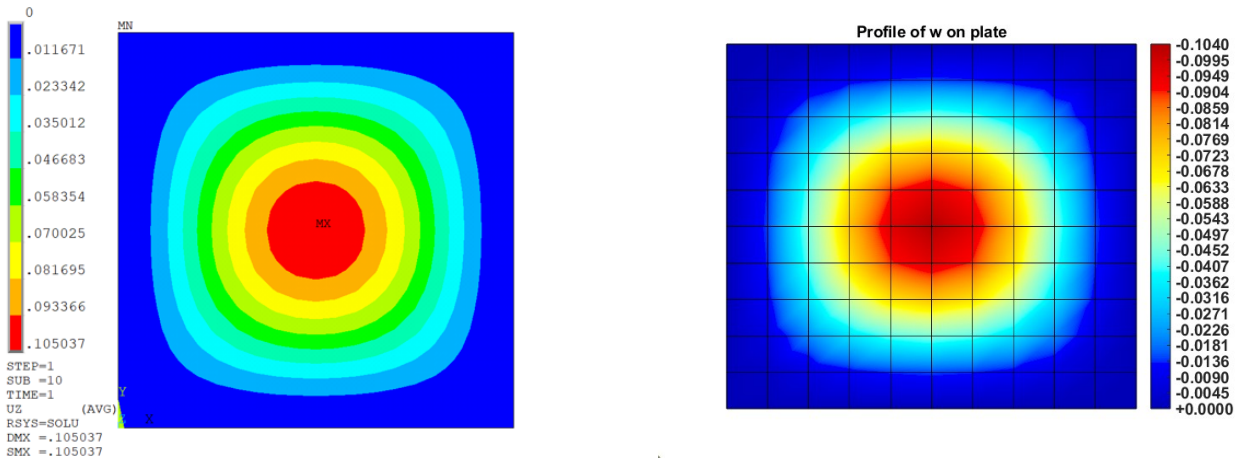

(a) **(b)**

Fig. 4 Displacement fields of the clamped plate acted upon by uniform pressure of 1 MPa: a) ANSYS; b) in-house code

B. Propagation of Microstructural Uncertainty on Macro-Scale under Isotropic Material Consideration

In this section, we explore the uncertainty propagation from the micro-scale to the macro-scale properties, assuming that the material is isotropic. This means that in FE analysis, each element is treated as isotropic, with uniform properties ($E_{11} = E_{22} = E_{33}$, $\nu_{12} = \nu_{13} = \nu_{23}$, and $G_{12} = G_{13} = G_{23}$). The only variables we control are the modulus of elasticity and Poisson's ratio, which are selected from their respective distributions. The FE analysis described is then employed to determine the distribution of the global deflection.

Additionally, due to the material's isotropy, we can derive the analytical solution for the maximum deflection based on previous studies, allowing us to accurately assess the deflection distribution. Equation (8) describes the deflection $u(x, y)$ of a simply-supported square plate under a uniformly distributed load, p. The double summation represents a Fourier sine series accounting for the plate's mode shapes in both the x- and y-directions. The deflection is influenced by the bending rigidity, $D = \frac{Eh^3}{12(1-\nu^2)}$, and higher modes contribute less due to the rapidly increasing denominator. The sine terms enforce the boundary condition that the deflection is zero along the edges, with the largest deflection occurring at the center of the plate. For this instance, the values of m and n are considered up to 201 to ensure the analytical deflection calculation reaches sufficient convergence.

$$u(x, y) = \frac{16p}{\pi^6 D} \sum_{m=1,3,5,\ldots}^{\infty} \sum_{n=1,3,5,\ldots}^{\infty} \frac{\sin\left(\frac{m\pi x}{L_x}\right) \sin\left(\frac{n\pi y}{L_y}\right)}{mn\left[\left(\frac{m}{L_x}\right)^2 + \left(\frac{n}{L_y}\right)^2\right]^2} \tag{8}$$

Before plotting the distribution of deflections, a visualization of the maximum and minimum deflections at each node of the square plate is presented. These deflections result from the variations in the elastic moduli and Poisson's ratio, which are sampled from the distributions at the meso-scale. Also, the Gaussian distribution was identified previously at the meso-scale work of Billah and Acar [6]. Fig. 6 illustrates the deformed shape of the plate, emphasizing the points of maximum and minimum deflection across the structure. This provides an intuitive representation of the localized effects of uncertainty propagation at the macro-scale, enabling us to better understand the deflection distribution before diving into statistical comparisons.

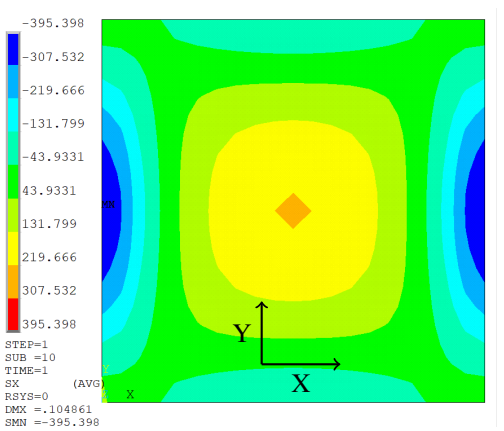

(a) Stress along X direction (S1, MPa) by ANSYS

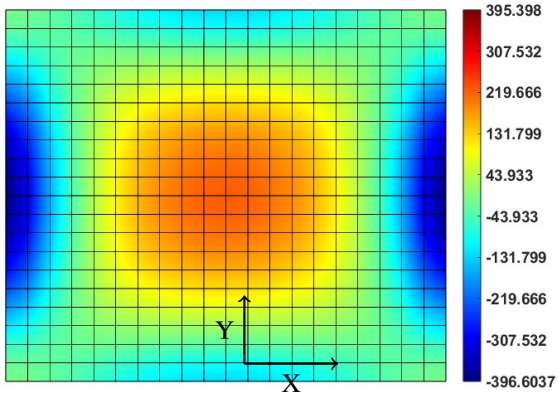

(b) Stress along X direction (S1, MPa) by in-house code

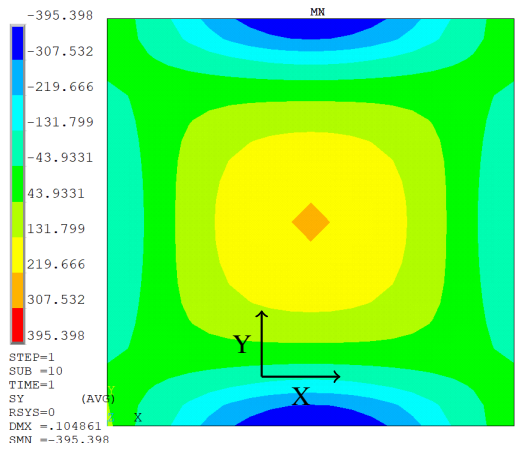

(c) Stress along Y direction (S2, MPa) by ANSYS

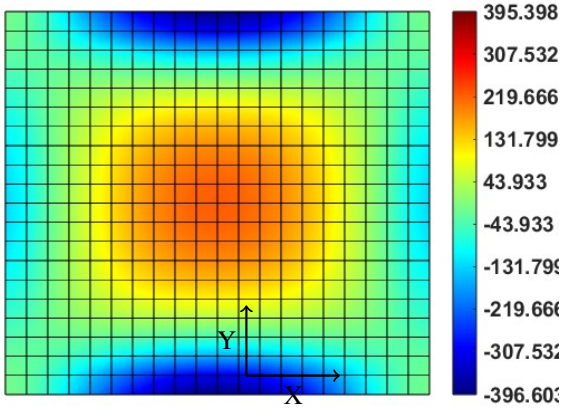

(d) Stress along Y direction (S2, MPa) by in-house code

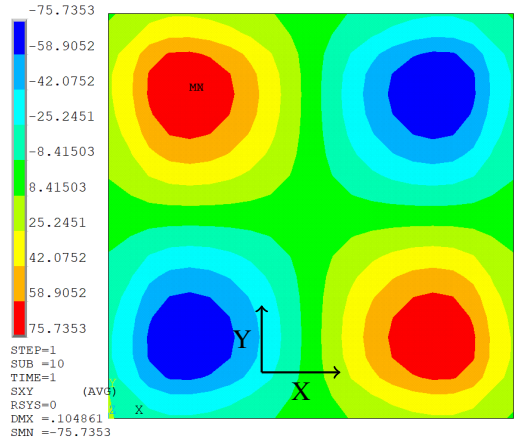

(e) Shear stress along XY direction (S12, MPa) by ANSYS

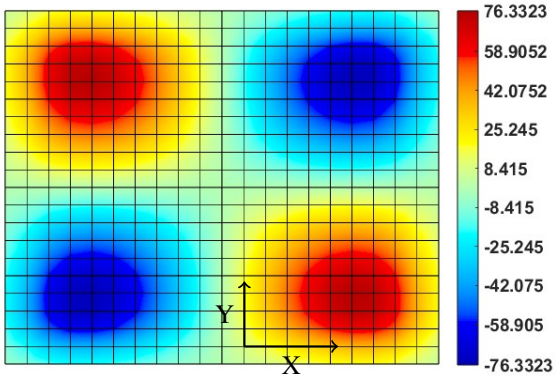

(f) Shear stress along XY direction (S12, MPa) by in-house code

Fig. 5 Stresses of the clamped plate acted upon by uniform pressure of 1 MPa: a), c), e) corresponds to results from ANSYS, whereas b), d), f) corresponds to results from the in-house code.

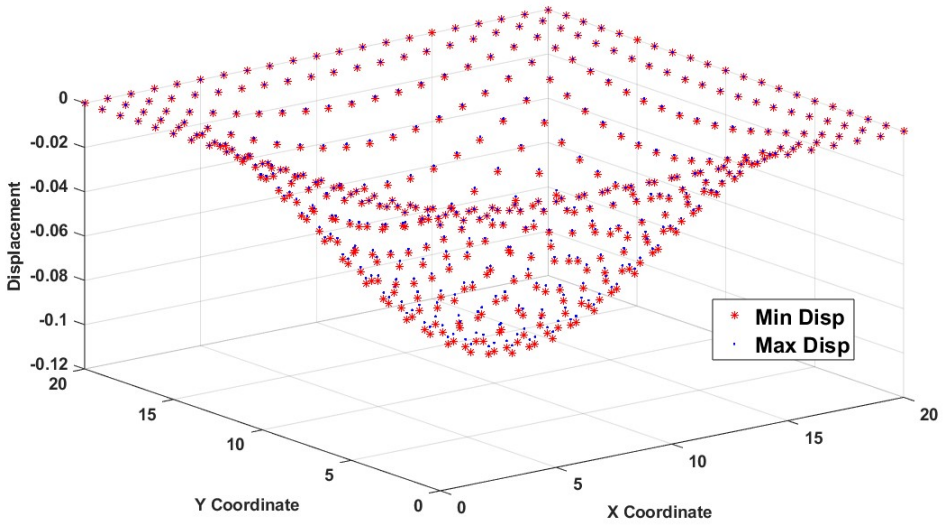

Fig. 6 Minimum and maximum deflection of at each node of fixed plate acted upon by a pressure of 1MPa out of all the 100000 samples

Fig. 7 depicts the comparison between analytical and FEM results, where the mean and standard deviation of elastic moduli and Poisson's ratio of Ti-7Al microstructures are 167.2841 GPa and 4.3345 GPa, and 0.33 and 0.008547, respectively, as adopted from a preceding study [6]. Monte Carlo Sampling is used to generate 100,000 random samples, allowing for a comprehensive exploration of the variability in input parameters. Both analytical and FE calculations are then performed on these samples to obtain histograms of the properties, such as maximum deflection, providing a statistical distribution of the results. This comparative analysis reveals that the distributions are nearly symmetric and closely aligned, demonstrating the accuracy of the proposed FE model in capturing the solution. However, the uncertainty in deflection may not exhibit a symmetric distribution due to variability in material properties. Specifically, larger standard deviations in elastic moduli and Poisson's ratio can distort the shape of the distribution, causing the deflection's frequency distribution to become left and right skewed, respectively, due to the non-linear relationship between these parameters and deflection. In other words, relatively higher uncertainty in the elastic moduli leads to a left-skewed histogram, whereas higher uncertainty in Poisson's ratio results in a right-skewed histogram. A balanced uncertainty between these two parameters, or lower uncertainty in both, produces a more symmetric histogram.

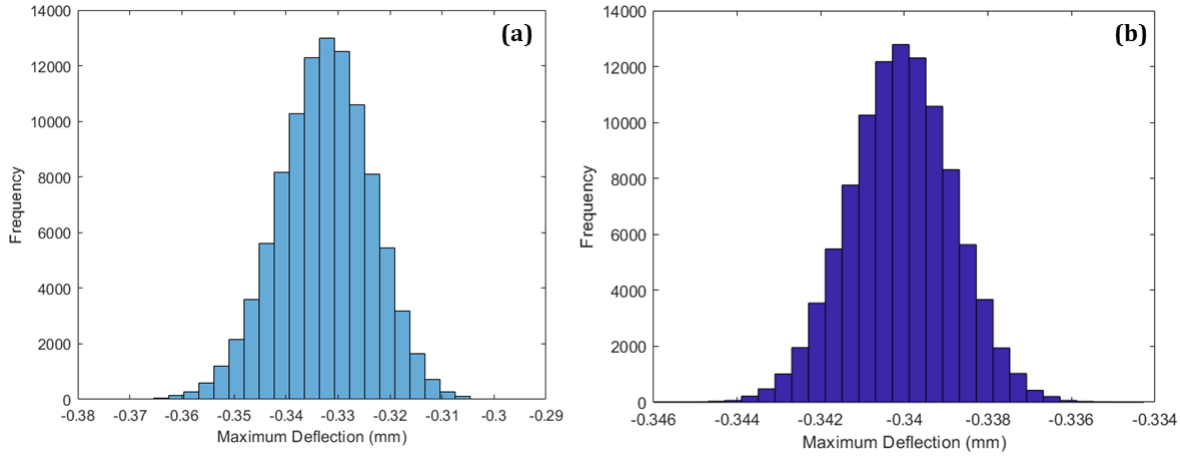

Fig. 7 Distribution of maximum stress for isotropic material consideration with uniformly distributed 1 MPa load and simply-supported boundary condition using 100, 000 samples, obtained from (a) Analytical solution (b) FE analysis.

C. Propagation of Microstructural Uncertainty on Displacement and Stress Fields of an Orthotropic Plate

After studying the propagation of uncertainty in an isotropic plate and verifying the results with analytical solutions, we extend our investigation to the propagation of uncertainty over the deflections and stresses of a transversely loaded, simply-supported orthotropic square plate. This means that each element of the FE model is considered as orthotropic. To determine the elasticity tensor, Q, for each element in the plate's FE model, the following steps are performed:

- The elastic moduli (E) along the 1 and 2 directions are sampled from distributions given by Billah and Acar [6].
- The distribution of ν is considered similar to the distribution of E, i.e., the ratio of standard deviation of ν to the mean value of ν is the same as the ratio of standard deviation of E to the mean value of E.
- The elasticity tensor of the i^{th} element for the j^{th} design sample, $Q^{(i,j)}$, is defined as:

$$Q^{(i,j)} = \begin{bmatrix} \frac{E_1^{(i,j)}}{1-\nu_{12}^{(i,j)}\nu_{21}^{(i,j)}} & \frac{\nu_{12}^{(i,j)}E_2^{(i,j)}}{1-\nu_{12}^{(i,j)}\nu_{21}^{(i,j)}} & 0 \\ \frac{\nu_{21}^{(i,j)}E_1^{(i,j)}}{1-\nu_{12}^{(i,j)}\nu_{21}^{(i,j)}} & \frac{E_2^{(i,j)}}{1-\nu_{12}^{(i,j)}\nu_{21}^{(i,j)}} & 0 \\ 0 & 0 & G^{(i,j)} \end{bmatrix}$$

where $E_1^{(j)}$ and $E_2^{(j)}$ are the j^{th} random samples drawn from the normal distributions defined for E_1 and E_2, with means of 167.2841 GPa and standard deviations of 4.3345 GPa.
$\nu_{12}^{(j)}$ is the j^{th} random sample from a normal distribution with a mean of 0.33 and a standard deviation of 0.008547. The other material properties are obtained as follows: $\nu_{21}^{(j)} = \frac{E_2^{(j)}}{E_1^{(j)}}\nu_{12}^{(j)}$, and $G^{(j)} = \frac{E_1^{(j)}E_2^{(j)}}{E_1^{(j)}+2\nu_{12}^{(j)}E_1^{(j)}+E_2^{(j)}}$ [27]

The FE model of the transversely loaded, simply-supported square plate is constructed with a different elasticity tensor for each element. FE simulations are conducted for each sample using Monte Carlo sampling approach to obtain the uncertainties of displacements and stresses.

To study how different distributions of E and ν influence the resulting distributions of stresses and deflections, four distinct cases are designed, each exploring a unique combination of variability in these material properties.

In the first scenario, FE simulations are performed with prescribed distributions of E and ν, allowing us to assess the mean and standard deviation values of deflections and stresses. Figure 8 illustrates the distributions for deflection and stress results. The deflection distribution (Fig. 8a) highlights the maximum value of deflection, while the maximum stress distribution along the 1-direction (Fig. 8b) emphasizes the impact of orthotropic material properties on stress.

The second case introduces increased variability in E, with a fixed ν. Here, the uncertainty in E significantly affects both displacement and stress fields, as observed in Fig. 9. Maximum deflection and stress along the X-axis reflect the effect of heightened variability in material stiffness, yielding distributions of deflection and stress with higher variations.

The third scenario examines the influence of increased variability in ν while holding E constant. This variation primarily affects the material's lateral strain response, modifying deflection and stress distributions as shown in Fig. 10. With increased ν variability, lateral strain adjustments lead to a non-uniform spread of deflection and stress fields across the plate.

In the final case, we increase variability in both E and ν simultaneously, creating a complex response pattern in the plate, shown in Fig. 11. The combination of both uncertain parameters results in broader, more dispersed distributions of both deflection and stress. This integrated approach highlights the importance of accurately representing property distributions in FE models to capture the sensitivity of orthotropic materials effectively.

These results given in Table 1 highlights the role of variability in E and ν in affecting the structural response, emphasizing the importance of comprehensive UQ for reliable FE modeling of orthotropic materials.

Table 1 Mean and standard deviation of deflections and stresses for the four scenarios of distribution of E and ν considered

Scenarios	Max. Deflection, mm		Max stress in X, MPa	
	Mean(μ)	Std. Deviation(σ)	Mean(μ)	Std. Deviationσ
Scenario 1	-0.3380	0.0010	465.1850	4.2856
Scenario 2	-0.3400	0.0046	477.0468	16.1082
Scenario 3	-0.3295	0.0106	483.9022	186.5576
Scenario 4	-0.3312	0.0117	498.0338	296.8581

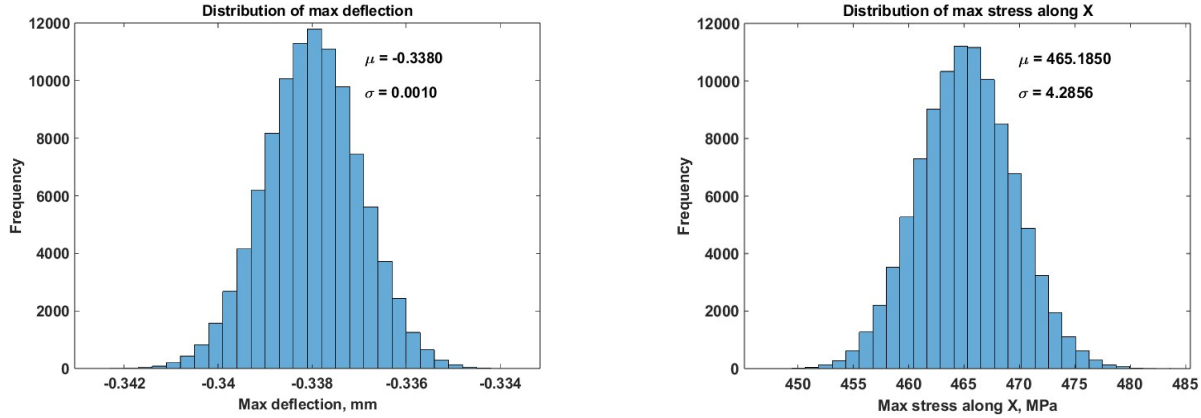

(a) (b)

Fig. 8 Distribution of stresses and maximum deflection in a simply-supported orthotropic plate under uniform pressure of 1 MPa and given E and ν distribution: a) Maximum deflection (mm); b) Stress along X direction (MPa)

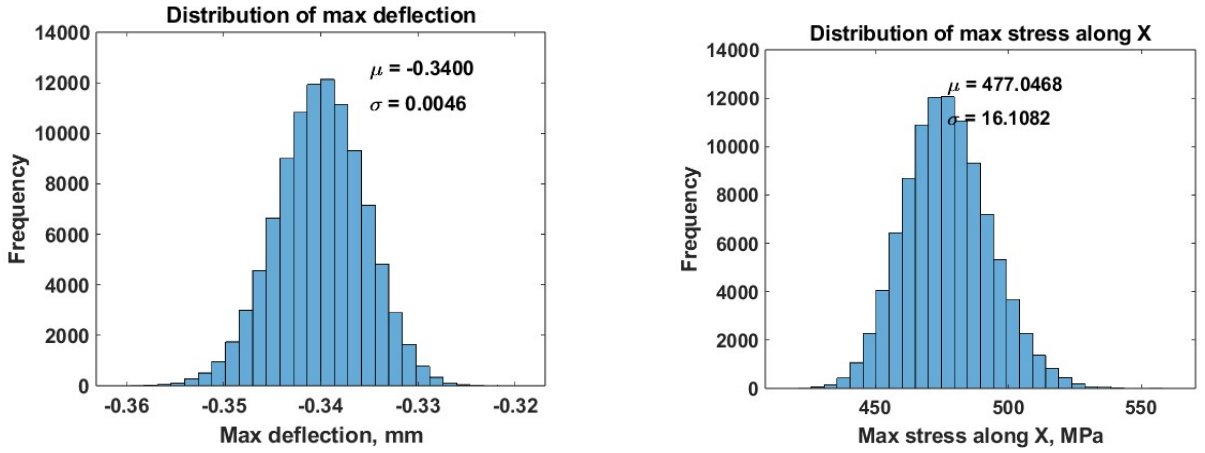

(a) (b)

Fig. 9 Distribution of stresses and maximum deflection in a simply-supported orthotropic plate under uniform pressure of 1 MPa with increased variability in E and given ν distribution: a) Maximum deflection (mm); b) Stress along X direction (MPa)

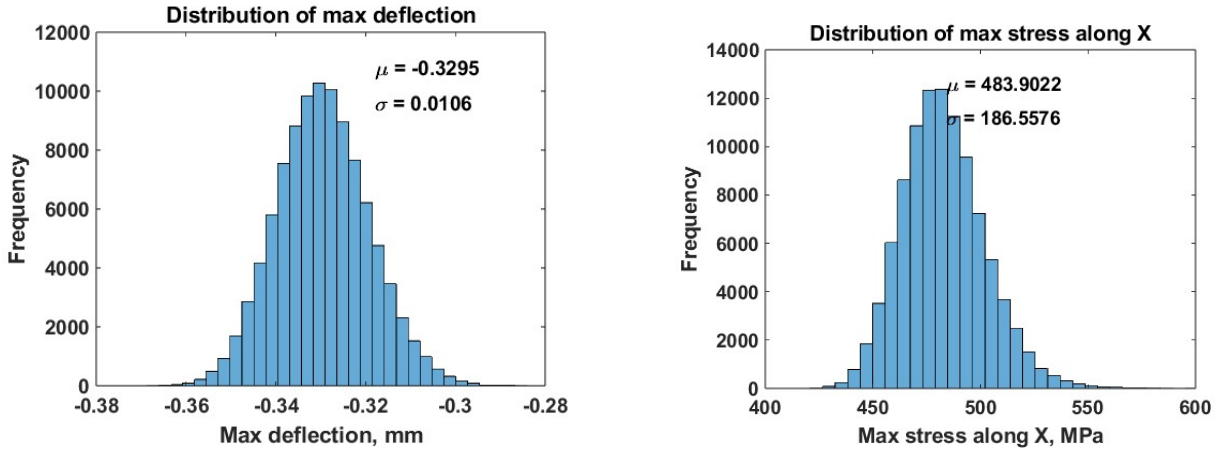

(a) (b)

Fig. 10 Distribution of stresses and maximum deflection in a simply-supported orthotropic plate under uniform pressure of 1 MPa with given E and increased variability ν distribution: a) Maximum deflection (mm); b) Stress along X direction (MPa)

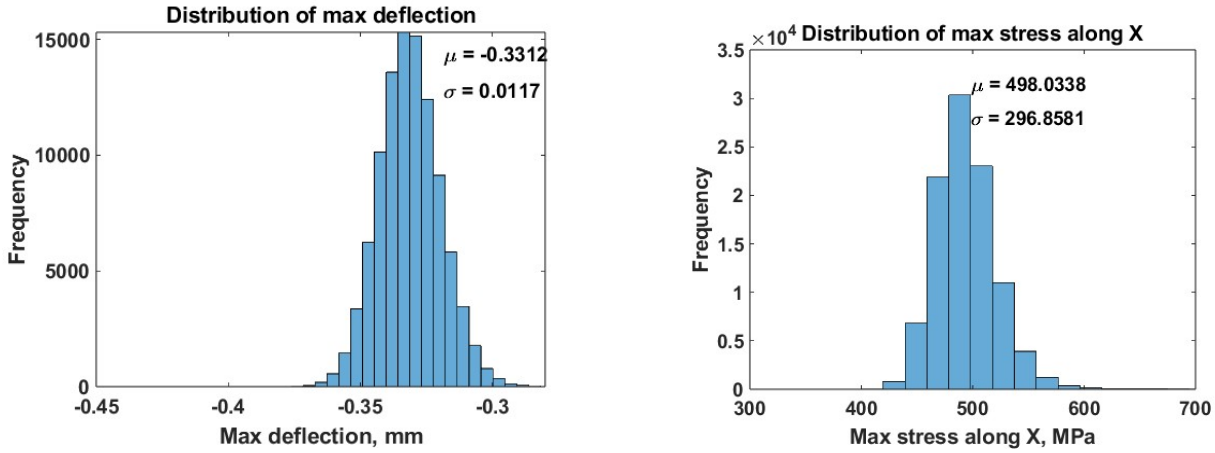

(a) (b)

Fig. 11 Distribution of stresses and maximum deflection in a simply-supported orthotropic plate under uniform pressure of 1 MPa with increased variability in both E and ν distribution: a) Maximum deflection (mm); b) Stress along 1 direction (MPa)

IV. Conclusion

This study develops a framework to assess the influence of microstructural uncertainties on the mechanical properties of Ti-7Al alloy at meso- and macro-scales. By incorporating stochastic variations in elastic modulus and Poisson's ratio, the framework effectively captures the propagation of uncertainty from microstructural level to the component-level (macroscopic level) responses. Validation against analytical and FE solutions demonstrates a closed agreement, underscoring the robustness of the custom finite element model in studying mechanical behavior.

The results show that microstructural uncertainties impact stress and displacement distributions of the alloy, indicating the necessity of accounting for such variability in the design of aerospace components. Variations in elasticity tensor lead to observable shifts in deflection and stress distributions, with different uncertainty levels resulting in different patterns in deflection and stress variations. This highlights the necessity that microstructural variability should be integrated into engineering design and analysis to maintain structural integrity and reliability.

Future work will expand this methodology to account for complex loading scenarios and anisotropic behavior in other aerospace alloys.

Acknowledgments

The authors acknowledge funding from the National Science Foundation (NSF) (CMMI Awards # 2053840 and # 2328112) and support through the Future Additive Interdisciplinary Manufacturing (FAIM) project supported under the National Defense Education Program of the Office of Naval Research (ONR).

References

[1] Boyer, R., "Titanium for aerospace: rationale and applications," *Advanced Performance Materials*, Vol. 2, 1995, pp. 349–368.

[2] Singh, P., Pungotra, H., and Kalsi, N. S., "On the characteristics of titanium alloys for the aircraft applications," *Materials today: proceedings*, Vol. 4, No. 8, 2017, pp. 8971–8982.

[3] Thillaithevan, D., Bruce, P. J., and Santer, M. J., "Modelling material uncertainty in multiscale optimization using lattice microstructures," *AIAA Scitech 2021 Forum*, 2021, p. 1593.

[4] Hasan, M., and Acar, P., "Uncertainty quantification of metallic microstructures with analytical and machine learning based approaches," *AIAA Journal*, Vol. 60, No. 1, 2022, pp. 461–472.

[5] Sofi, A., and Romeo, E., "A unified response surface framework for the interval and stochastic finite element analysis of structures with uncertain parameters," *Probabilistic Engineering Mechanics*, Vol. 54, 2018, pp. 25–36.

[6] Billah, M. M., and Acar, P., "Design of polycrystalline metallic alloys under multi-scale uncertainty by connecting atomistic to meso-scale properties," *Acta Materialia*, Vol. 270, 2024, p. 119879.

[7] Acar, P., and Sundararaghavan, V., "Uncertainty quantification of microstructural properties due to variability in measured pole figures," *Acta Materialia*, Vol. 124, 2017, pp. 100–108.

[8] Ding, J., Zheng, H.-r., Tian, Y., Huang, X., Song, K., Lu, S.-q., Zeng, X.-g., and Ma, W.-S., "Multi-scale numerical simulation of fracture behavior of nickel-aluminum alloy by coupled molecular dynamics and cohesive finite element method (CFEM)," *Theoretical and Applied Fracture Mechanics*, Vol. 109, 2020, p. 102735.

[9] Acar, P., "Uncertainty quantification for Ti-7Al alloy microstructure with an inverse analytical model (AUQLin)," *Materials*, Vol. 12, No. 11, 2019, p. 1773.

[10] Acar, P., Ramazani, A., and Sundararaghavan, V., "Crystal plasticity modeling and experimental validation with an orientation distribution function for ti-7al alloy," *Metals*, Vol. 7, No. 11, 2017, p. 459.

[11] Acar, P., "Design optimization of metallic alloy microstructures under epistemic uncertainty," *AIAA Scitech 2020 Forum*, 2020, p. 0884.

[12] Tran, A., Robbe, P., and Lim, H., "Multi-fidelity microstructure-induced uncertainty quantification by advanced Monte Carlo methods," *Materialia*, Vol. 27, 2023, p. 101705.

[13] Kamiński, M., "Uncertainty analysis in solid mechanics with uniform and triangular distributions using stochastic perturbation-based Finite Element Method," *Finite Elements in Analysis and Design*, Vol. 200, 2022, p. 103648.

[14] Stefanou, G., "The stochastic finite element method: past, present and future," *Computer methods in applied mechanics and engineering*, Vol. 198, No. 9-12, 2009, pp. 1031–1051.

[15] Li, Z., Pasternak, H., and Geißler, K., "Buckling Analysis of Cylindrical Shells using Stochastic Finite Element Method with Random Geometric Imperfections," *ce/papers*, Vol. 5, No. 4, 2022, pp. 653–658.

[16] Cheng, S., Quilodrán-Casas, C., Ouala, S., Farchi, A., Liu, C., Tandeo, P., Fablet, R., Lucor, D., Iooss, B., Brajard, J., et al., "Machine learning with data assimilation and uncertainty quantification for dynamical systems: a review," *IEEE/CAA Journal of Automatica Sinica*, Vol. 10, No. 6, 2023, pp. 1361–1387.

[17] Muhanna, R. L., and Shahi, S., "Uncertainty in boundary conditions—an interval finite element approach," *Decision Making under Constraints*, 2020, pp. 157–167.

[18] Sedehi, O., Papadimitriou, C., and Katafygiotis, L. S., "Hierarchical Bayesian uncertainty quantification of Finite Element models using modal statistical information," *Mechanical Systems and Signal Processing*, Vol. 179, 2022, p. 109296.

[19] McKenna, F., Yi, r., Aakash, B., Zsarnoczay, A., Gardner, M., and Elhaddad, W., "NHERI-SimCenter/quoFEM: Version 3.2. 0 (v3. 2.0)," , 2022.

[20] Ghanem, R., "Hybrid stochastic finite elements and generalized Monte Carlo simulation," 1998.

[21] Liu, J. S., and Liu, J. S., *Monte Carlo strategies in scientific computing*, Vol. 10, Springer, 2001.

[22] Xiu, D., and Hesthaven, J. S., "High-order collocation methods for differential equations with random inputs," *SIAM Journal on Scientific Computing*, Vol. 27, No. 3, 2005, pp. 1118–1139.

[23] Dannert, M. M., Bensel, F., Fau, A., Fleury, R. M., and Nackenhorst, U., "Investigations on the restrictions of stochastic collocation methods for high dimensional and nonlinear engineering applications," *Probabilistic Engineering Mechanics*, Vol. 69, 2022, p. 103299.

[24] Służalec, A., "Simulation of stochastic metal-forming process for rigid-viscoplastic material," *International journal of mechanical sciences*, Vol. 42, No. 10, 2000, pp. 1935–1946.

[25] Doltsinis, I., "Inelastic deformation processes with random parameters—-methods of analysis and design," *Computer methods in applied mechanics and engineering*, Vol. 192, No. 20-21, 2003, pp. 2405–2423.

[26] Chen, D.-C., You, C.-S., Nian, F.-L., and Guo, M.-W., "Using the Taguchi method and finite element method to analyze a robust new design for titanium alloy prick hole extrusion," *Procedia Engineering*, Vol. 10, 2011, pp. 82–87.

[27] Urban, F., and Middendorf, P., "Macroscopic Modeling of the Linear Viscoelastic Vibration Behavior of Short Fiber Reinforced Plastics," *SAMPE 2020| Virtual Series*, 2020.